ARTICLE

Facet-dependent growth of InAsP quantum wells in InP nanowire and nanomembrane array

Received 00th January 20xx,
Accepted 00th January 20xx

DOI: 10.1039/x0xx00000x

Xiaoming Yuan[a, *, #], Naiyin Wang[b, #], Zhenzhen Tian[a], Fanlu Zhang[b], Li Li[c], Mark Lockrey[d], Jun He[a, *], Chennupati Jagadish[b, e] and Hark Hoe Tan[b, e]

Selective area epitaxy is a powerful growth technique that has been used to produce III-V semiconductor nanowire and nanomembrane arrays for photonic and electronic applications. The incorporation of heterostructure such as quantum wells (QWs) brings new functionality and further broadens their applications. Using InP nanowire and nanomembrane as a template, we investigate the growth of InAsP QWs on these pure wurtzite nanostructures. InAsP QWs grow both axially and laterally on the nanowires and nanomembranes, forming a zincblende phase axially and wurtzite phase on the sidewalls. On non-polar $\{1\bar{1}00\}$ sidewalls, the radial QW selectively grows on one sidewall which locates at the semi-polar $<11\bar{2}>$A side of the axial QW, causing the shape evolution of the nanowires from hexagonal to triangular cross section. For nanomembranes with $\{1\bar{1}00\}$ sidewalls, radial QW grows asymmetrically on the $\{1\bar{1}00\}$ facet, destroying their symmetry. In comparison, nanomembranes with $\{11\bar{2}0\}$ sidewalls are shown to be an ideal template for InAsP QW growth thanks to the uniform QW formation. These QWs emit strongly in the near IR region at room temperature and their emission can be tuned by changing the QW thickness or composition. These findings enrich our understanding in the growth of QWs which provides new insights for heterostructure design in other III-V nanostructures.

Introduction

Bottom-up epitaxy of III-V semiconductor nanostructures has produced a diverse range of "building-blocks" for photonic and optoelectronic device applications.[1,2] Among all the synthesis methods, selective area epitaxy (SAE) is of great interests thanks to its unbeatable advantages in producing uniform nanostructure arrays with controllability in pattern geometry, such as diameter and site position.[3,4] Indeed SAE has been used to grow nanowires for solar cells[5,6] and light emitting diodes.[7] In addition to nanowire arrays, several research groups have successfully fabricated other III-V semiconductor nanoshape arrays, such as nanomembranes, nanorings and in-plane nanowire arrays,[8-12] which may provide new functionalities. Furthermore, SAE has been used to fabricate InAs and InSb nano-networks that are required for realizing topologically protected majorana-based qubits.[13-16] Based on the principle of SAE, IBM researchers and Borg et al. developed a template-assisted method to realize integration of III-V nanostructures on silicon substrates, and demonstrated state-of-the-art field effect transistors and GaAs microdisk lasers.[17-19] These advances show the potential to monolithically integrate III-V nanostructures with matured silicon CMOS processes to achieve devices with better optical and electronic properties. Moreover, researchers have also combined metal-catalysed growth with SAE by incorporating the catalyst into the pattern openings to achieve more flexibility in growth. By this so-called SA vapor-liquid-solid approach, growth conditions can be easily tuned to form axial[20-22], lateral[23,24] nanowire heterojunctions and even nanowire networks.[25,26] These achievements demonstrate that SAE is of interest to produce nanostructure and network arrays for the future photonic, electronic and quantum science applications.

The incorporation of QW and quantum dot (QD) is vital to improve the properties and functionality of III-V semiconductors. For instance, the axially embedded QD in nanowires have high emission efficiency thanks to the natural Fabry–Pérot cavity of nanowire themselves, and widely applied in lasing[27], single photon emission[23,28] and infrared photodetection applications.[29] However, despite the great success in SAE of homogeneous III-V nanostructure arrays, heterostructure formation is less studied. Here, InP is chosen for heterostructure growth in consideration of its unique properties among the III-V semiconductors and well-accumulated growth knowledge in both nanowire and nanomembrane forms. SAE of InP nanostructures was pioneered by Fukui et al.[4]with the focus on nanowires, and been further developed by Wang et al.[9]and Staudinger et al.[30,31]to achieve pure WZ InP nanomembrane, nanoring and microdisk arrays[9,32] for applications in various fields.[5,33-36] In comparison, the SAE of InP-based heterojunction is less investigated. Yang et al. observed the formation of QW and shape evolution during SAE of InP/InGaAs nanowires.[37] Han et al. demonstrated the in-plane InP/InGaAs QW nanowire array lasers grown on silicon substrate.[38] Mohan et al. successfully grew InP/InAs QW nanowire array by changing the growth conditions to promote lateral growth.[39] Compared with the well-studied metal-catalysed InP/InAsP and InP/InGaAs QD

[a] Hunan Key Laboratory of Super Microstructure and Ultrafast Process, School of Physics and Electronics, Central South University, Changsha, Hunan 410083, P. R. China.
[b] Department of Electronic Materials Engineering, Research School of Physics, The Australian National University, Canberra, ACT 2601, Australia.
[c] Australian National Fabrication Facility ACT Node, Research School of Physics and Engineering, The Australian National University, Canberra, ACT 2601, Australia.
[d] Microstructural Analysis Unit, University of Technology Sydney, Sydney, NSW 2007, Australia.
[e] ARC Centre of Excellence for Transformative Meta-Optical Systems, Research School of Physics, The Australian National University, Canberra, ACT 2601, Australia.
# These authors contributed equally to this work.
* Corresponding authors: xiaoming.yuan@csu.edu.cn; hejun@csu.edu.cn
Electronic Supplementary Information (ESI) available: [details of any supplementary information available should be included here]. See DOI: 10.1039/x0xx00000x

nanowires[21,29, 40-43], the development of SAE based heterostructure is slower due to the more growth challenging, as it is harder to selectively control axial and lateral growth rates by only tuning the growth conditions without the help of a catalyst. This situation leads to the insufficient understanding of heterostructure incorporation. Recently, with the increasing interests in nanoshape and network structures, the growth understanding gained from nanowire research should be enhanced.

In this work, using our previously optimized pure WZ InP nanowire and nanomembrane arrays as a template, we investigate the growth behaviour of InAsP QW, including the crystal structure, morphology, polarity and composition. We reveal an asymmetric growth of InAsP on non-polar $\{1\bar{1}00\}$ sidewalls. In comparison, InAsP growth on InP $\{11\ \bar{2}\ 0\}$ sidewalls is quite uniform whilst maintaining the morphological symmetry of the $<11\bar{2}>$-oriented nanomembranes. Bright emission is observed from the nanomembrane QW heterostructures.

Results and discussion

Typical morphology and structure of the InP/$InAs_{0.15}P_{0.85}$ QW nanowires are shown in Figure 1. These QW nanowire arrays can be formed with a broad range of diameters. The diameter can be reduced to as small as ~40 nm which is a requirement for single photon emitters.[28] The position of the $InAs_{0.15}P_{0.85}$ QW can be easily spotted due to the discontinuity of the side facets, as indicated by the red arrow in Figure 1b. For nanowires with a large diameter, scanning electron microscopy (SEM) images show that most of them have a uniform triangle-like cross-section. No facet rotation induced by QW growth is observed.[37] The triangular morphology of InP/InAsP QW nanowire is also true for other investigated QW growth conditions (See Figure S1). Normally, the non-polar nature of WZ nanowire sidewalls leads to a hexagonal shape for InP nanowires, as demonstrated previously[9] and in Figure S2. Therefore, it is suggested that InAsP QW growth causes the morphology transformation from hexagonal to triangular shape, as also observed in InP/InAs core/shell nanowire array. [44] Thickness resolved high-angle annular dark-field (HAADF) image analysis demonstrates that the InP/InAsP QW nanowire sidewalls are still non-polar $\{1\bar{1}00\}$ (see analysis in Figure S1f). After InAsP QW growth, the diameter of the top InP segments becomes smaller. This is caused by the shrinkage of the {111}A facet area due to the formation of inclined side facets during InAsP QW growth (see Figure 1c). The InAsP QW growth alters the following InP growth. The axial growth rate of InP is reduced by a factor of 2.2±0.2 after the QW growth, which could be due to an increased competition of lateral growth.

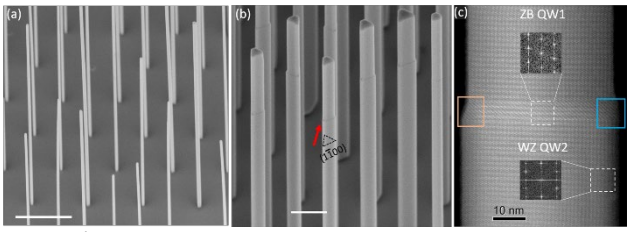

Fig.1 InP/InAsP QW nanowire array. 45° tilted SEM images of InP/$InAs_{0.15}P_{0.85}$ QW nanowire arrays with different diameters: (a) ~55 nm (b) ~200 nm. (c) Low magnification HAADF image of a QW nanowire with small diameter (48 nm) along the $[11\bar{2}0]$ zone axis. The scale bars are 1 µm in (a, b).

Z-contrast HAADF image in Figure 1c shows the structure of QW nanowire. The InAsP regions look brighter than the InP matrix due to the heavier As element. Despite the optimized growth conditions for axial growth, both axial and lateral InAsP QWs are observed, which are confirmed to be ZB and WZ phase by fast Fourier transform (FFT) analysis in the insets, respectively. The formation of both axial and radial QWs in InP nanowires grown by SAE has been observed in InP/InGaAs[37,45] and InP/AlInP systems.[46] The simultaneous incorporation of both axial and radial QW makes the SAE of purely axial or radial nanowires challenging, and therefore a thorough understanding of the growth behaviour would be highly valuable.

Atomically resolved HAADF images in Figure 2a-b show the details of the $InAs_{0.15}P_{0.85}$ QW structure. Axially, InAsP QW forms a ZB phase with (111)A polarity and the crystal phase of the top InP segment switches back to WZ phase immediately after InAsP QW growth, thus forming an atomically sharp interface between ZB InAsP QW and WZ InP. The axial InAsP QW forms inclined {111}B side facets, suggesting that the stable polarity of InAsP (111) facet is B-polar. The growth of InAsP along <111>A direction is not stable and cannot be maintained after a long growth time (see Figure S3), since InAsP nanowire prefers to grow along <111>B-polar direction.[29] These inclined side facets lead to a morphological discontinuity between the two InP segments and hence easy identification of the axial QW position as observed in Figure 1b. The other side facets of the InAsP QW consist of vertical $\{11\bar{2}\}$A (as determined by FFT of ZB QW [47]) and a small inclined facet. The atomic arrangement between the InAsP QW and InP is schematically illustrated in Figure 2c. Below the axial QW in Figure 2b, the lateral QW growth inherits the WZ stacking sequence of the InP nanowire. The three-dimensional distribution of InAsP is revealed by energy dispersive X-ray (EDX) mapping in Figure 2d, e. The intensity of P element is slightly stronger on left-hand side of the nanowire due to a thicker region, confirming the triangle-like cross-section. Strong As element signal is detected at both the axial QW position and near the right-hand edge of the nanowire, demonstrating the formation of radial InAsP QWs along the nanowire. Moreover, a weaker As signal can also be seen on the left-hand (thicker region) of the nanowire. Considering the crystal symmetry, HAADF, EDX and SEM results suggest that three InAsP radial QWs are formed on the $\{1\bar{1}00\}$ sidewalls, as illustrated by the 3D schematic images in Figure 2f.

Facet-selective growth has been widely observed during heterostructure formation due to the differences in the surface energies and polarity.[48,49] Thus, the asymmetric growth for the radial InAsP QW observed above is unexpected since the $\{1\bar{1}00\}$ side facets of the InP nanowire are non-polar. The only polar sidewalls in this InP/InAsP QW nanowire system is the $\{11\bar{2}\}$ sidewalls of ZB axial InAsP QW. Taking this polarity into consideration, radial QW growth always locates on the $\{11\bar{2}\}$A polar side. (See more structure analysis in Figure S4), suggesting a common validity of this conclusion. The relation between the polarity of axial InAsP QW and asymmetric lateral QW growth is further discussed in InP/InAsP QW nanomembrane. The difference in surface property is one explanation for the shape evolution.[47] However, it only explains the side facet transformation from $\{1\bar{1}00\}$ to $\{11\bar{2}0\}$, which is not the case here. Yang et al. recently reported that the growth of ZB InGaAs QW could alter the growth of subsequent InP layer.[37] They observed a similar triangular-like radial InGaAs QW formation and attributed it to the fast nucleation rate in the ZB axial InGaAs QW which drove the lateral growth and shape evolution. The preference for $\{1\bar{1}0\}$ sidewalls in axial InGaAs QW finally led to facet rotation of subsequent InP growth, forming a hexagonal InP top with $\{11\bar{2}0\}$ facets.[37] However, in our case, the ZB axial InAsP QW growth seems to play a major role in affecting the lateral growth of the InP segment below the axial QW. The sidewalls for the whole nanowire maintain the same as $\{1\bar{1}00\}$ but the cross-section transforms from hexagonal to truncated-triangle after the growth of InAsP and the overlaying InP layer.

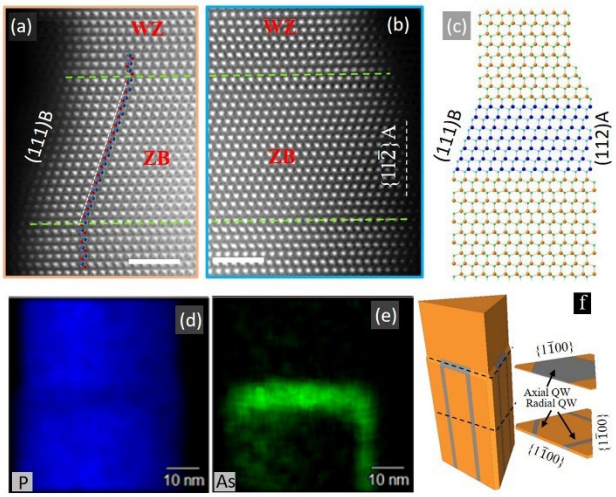

Fig.2 Detailed structural analysis of an InP/InAsP QW nanowire: (a-b) Atomically resolved HAADF images of the QW interface region as highlighted by the colored boxes in Figure 1. (c) Corresponding atomic model of the InP/InAsP QW nanowire. EDX mapping of (d) P and (e) As element. (f) Schematic illustration of the InP/InAsP QW nanowire with cross-sections showing the distribution of the axial and radial QWs. Scale bars are 2 nm in (a-b).

Since InP nanostructures grow along a different polarity in comparison to III-As and III-Sb compounds, a thorough understanding of InP/InAsP QW growth behavior is highly valuable. WZ InP nanowires grown by SAE lack the commonly observed {11$\bar{2}$0} facets. However, to fully understand the InAsP QW growth behavior, it is vital to investigate the growth of InAsP on different InP surfaces. Luckily, the recently reported pure WZ InP nanomembranes with mainly either {11$\bar{2}$0} or {1$\bar{1}$00} sidewalls[9] provides an ideal platform to investigate this. Figure 3 shows the growth of <1$\bar{1}$0>-oriented InP/InAsP QW nanomembranes. As reported in ref.[9], the InP nanomembrane array is very uniform and they have very smooth {1$\bar{1}$00} sidewalls. However, after the growth of InAsP QW, the nanomembrane array uniformity is reduced and the sidewalls appear not to be smooth. Cross-sectional lamellae were prepared by focused ion beam (FIB) milling along the white dotted line indicated in Figure 3a to expose the heterostructure interface. HAADF images along the [11$\bar{2}$0] zone axis (see Figure 3b-f) show that the QW formation is similar to that of the nanowires. Axially, InAsP is grown as a ZB phase while radially it grows as a WZ phase only on one {1$\bar{1}$00} sidewall. The radial QW grows along the <11$\bar{2}$>A-polar side of the axial QW. The radial QW thickness reduces from the top to the bottom of the nanomembrane (see more examples in Figure S5). Besides, the larger dimension of nanomembranes leads to new growth phenomenon. First, WZ InAsP is found to grow on (1$\bar{1}$02) facets of the InP nanomembrane (see Figure 3c), which is similar to that of InP/InGaAs nanowire heterostructure with larger diameters.[37] This is a result of the top {0001} facet not joining the {1$\bar{1}$00} sidewall at right angle, thus forming inclined {1$\bar{1}$02} facets. Subsequent growth of InP after the InAsP QW results in the formation of a thin ZB phase (~6.4 nm) before switching back to the preferred WZ phase (see Figure 3c). One possible explanation is the larger surface energy of InAsP {111}A facet than the {111}B facet leading to ZB nucleation instead of the normally observed WZ phase.[32] The lateral InP capping layer growth rate is also larger at the <11$\bar{2}$>A side of the axial InAsP QW (see more examples in Figure S5) in comparison to nearly zero growth rate along <11$\bar{2}$>B direction. This polarity driven growth rate difference is quite common in III-V nanowire heterostructure growth.[50] The WZ InP capping layer also prefers to grow faster along the <11$\bar{2}$>A direction. Moreover, this growth rate is larger when it is closer to the ZB section of the InP capping layer, leading to a thickness variation on the {1$\bar{1}$00} sidewall and the formation of inclined {1$\bar{1}$01} sidewalls. The above lateral WZ and ZB InP capping layer growth behavior in nanowires and nanomembranes suggest that the asymmetric lateral growth rate on non-polar {1$\bar{1}$00} facets could be related to the faster ZB InP growth on the semi-polar {11$\bar{2}$}A facets, which is similar to the InP/InGaAs QW nanowires.[37] Further increasing the number of InAsP QWs deteriorates the uniformity of the nanomembrane, forming a "protruding head" at one side of the nanomembrane (see Figure S6b). HAADF image of an InP/InAsP <1$\bar{1}$0>-orientated nanomembrane heterostructure with 5 QWs in Figure 3g shows the InAsP QW formation on the {0001}, {1$\bar{1}$00} and {1$\bar{1}$01} facets. The radial QWs are mostly formed on the <11$\bar{2}$>A sidewall but with a significant thickness nonuniformity. Moreover, the inclined {1$\bar{1}$01} facets consistently grow larger with the number of QWs, forming an irregular head as observed in SEM image of Figure S6b. An interesting point to note is that the axial growth rate is reduced to nearly zero after the first QW growth, most likely as a result of increased competition from lateral growth.

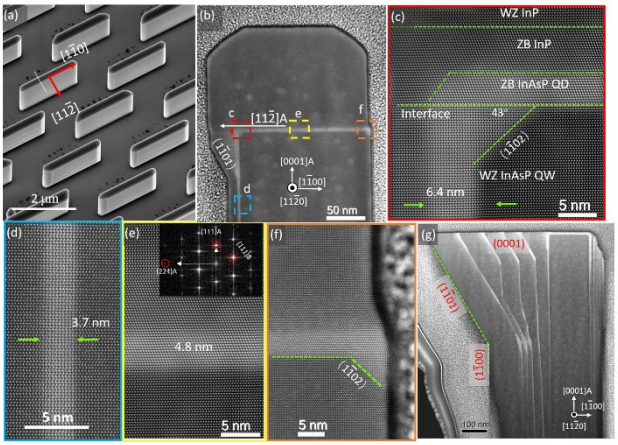

Fig.3 InAsP QWs grown on <1$\bar{1}$0>-orientated InP nanomembranes. (a) 30° tilted SEM image of the InP/InAsP QW nanomembrane array. The white dotted line indicates the ion milling direction for the TEM lamella preparation. (b) Cross-sectional HAADF image of the nanomembrane with one QW. (c-f) Atomically resolved HAADF images at different regions indicated by the colored boxes in (b) showing the crystal structure at the InP/InAsP interface. Inset in (e) is the FFT of the ZB InAsP axial QW. (g) Cross-sectional HAADF image of the InP nanomembrane with 5 InAsP QWs.

On the other hand, InAsP QW grown on the <11$\bar{2}$>-oriented InP nanomembranes is more uniform. No surface roughening is observed (see Figure 4a). HAADF image of the cross-section along [1$\bar{1}$00] zone axis in Figure 4b shows that the radial QWs grow on both {11$\bar{2}$0} sidewalls, forming a sharp interface with the InP matrix without any dislocation (see Figure 4d). The radial QW has a uniform thickness from the top to the bottom of the sidewalls with a thickness of ~2 nm. In comparison, the radial QW in Figure 3 has a thickness of 6.4 and 3.7 nm at the top and middle of the nanomembrane, respectively. Even after the growth of 5 InAsP QWs, the nanomembranes still maintain a good shape (see Figures 4c,e, S6c, S7a). In the <11$\bar{2}$>-oriented nanomembranes, axial growth rate of the QW is reduced significantly compared to the radial growth rate. Indeed, it may be even suppressed to nearly zero (see Figure S7b). These results show that {11$\bar{2}$0} facets are more desirable for multi-QW growth. The comparison of the InAsP QW composition in the two nanomembranes with different orientations are shown in Figure 4f,g. The As-element intensity maps show a relatively more uniform QW in the <11$\bar{2}$>-oriented membrane compared to the <1$\bar{1}$0>-oriented ones. The EDX spectra at different positions on the

nanomembranes are extracted for quantitative compositional analysis, as shown in Figure 4g. By comparing the intensity of the P-element with that from an InP reference sample, the InAsP composition in the QWs at locations 1-3 is determined to be $InAs_{0.63}P_{0.37}$, $InAs_{0.79}P_{0.21}$ and $InAs_{0.72}P_{0.28}$, respectively. The extracted composition difference between the axial and radial QWs for the $<1\bar{1}0>$-orientated nanomembrane is 16%, suggesting that QW composition is highly facet-dependent. The variation in composition could lead to different emission peaks and a complex emission behaviors. On the contrary, for the $<11\bar{2}>$-orientated InP nanomembrane, only radial QW is formed with uniform distribution.

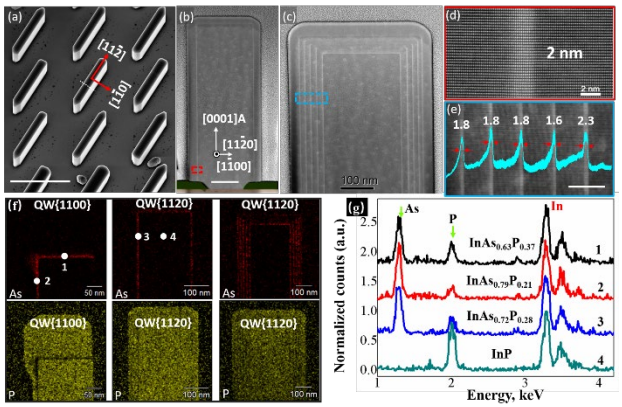

Fig.4 InAsP QWs grown on the $<11\bar{2}>$-oriented InP nanomembranes. (a) 30° tilted SEM image of the nanomembrane array with one InAsP QW. Low magnification HAADF images of the nanomembrane with a single (b) and five (c) InAsP QWs. The magnified HAADF images in (d) and (e) are taken from the boxed region in (b) and (c), respectively. (f) EDX maps of As and P from $<1\bar{1}0>$-oriented nanomembrane with one QW and $<11\bar{2}>$-orientated nanomembrane with one and five QWs. (g) EDX spectra taken at points 1-4 as indicated in (f). Scale bars are 2 μm in (a), 100 nm in (b) and 20 nm in (e).

The spatial-resolved optical properties of InP/InAsP QW nanowires and nanomembranes are studied by cathodoluminescence (CL), as shown in Figure 5. InP/InAsP QW nanowire (See Figure 5a) shows the strongest emission from the two ends of the nanowire due to a Fabry-Perot cavity.[32] Emission from WZ InP matrix is observe along the nanowire while the QW position shows a strong but broad emission peak from 900 to 1000 nm. The broad emission peak width from our QW nanowire is unexpected since the interface between InAsP and InP is quite sharp. One possible explanation is substantial composition fluctuation in the QW. Emission from the radial InAsP QW is not observed at room temperature most likely due to very thin layer of the QW which results in poor carrier confinement. The emission wavelength from the axial QW can be easily tuned by changing the QW growth time or composition (See Figure S8).

CL mapping was also performed on nanomembranes that have been knocked down from their growth substrate (InP) to evaluate the emission from the QW. Based on the fracture at the bottom (111) plane, the growth direction of the $<1\bar{1}0>$- and $<11\bar{2}>$-oriented InP/InAsP QW nanomembranes is represented by the green arrows in Figure 5e,i, respectively. For the $<1\bar{1}0>$-oriented nanomembrane, the CL emission spectra (see figure 5c) contain emissions from WZ InP (860~880 nm), radial QW (940~960 nm) and axial QW (1550~1570 nm). The emission map for these wavelength regions are shown in Figure 5f-h. The emission from WZ InP and radial QW have similar intensity distribution and is strongest at the lower half of the nanomembrane. At the top half section, the emission is dominated by the axial QW emission and the spectral range extends beyond 1.6 μm, which is the detection limit of our InGaAs detector. The observed emission wavelength and intensity of the axial and radial QWs vary from one nanomembrane to another due to the inhomogeneous thickness distribution and composition variation in QW (see Figure S9a-e for another example). In comparison, QW emission from the $<11\bar{2}>$-oriented nanomembrane is more uniform (see Figure 5j-l and Figure S9f-j). Fully avoiding of composition inhomogeneity in ternary InAsP QW could be challenging. Instead, using InAs to form InP/InAs QW structure could be an appropriate approach to obtain high-quality QW structure with both sharp interface and no composition difference. The signal from the WZ InP nanomembrane is fairly uniform across the whole nanomembrane. The radial QW emission spectrum can be deconvoluted into two peaks at 1280 and 1340 nm (Figure 5d). The intensity distributions of these two peaks are presented in Figure 5k-l, showing a similar spatial distribution trend. Except for the slightly stronger emission intensity at the right-hand side, QW emission is observed for the whole $\{11\bar{2}0\}$ facet. These results suggest a slight composition or thickness variation for the radial QW on the two $\{11\bar{2}0\}$ sidewalls. Even for different nanomembranes, QW emission distributes uniformly in the array, showing a strong and broad emission peak around 1.3 μm (see Figure S10). No axial QW related emission is observed from the $<11\bar{2}>$-oriented nanomembranes. These growth studies also suggest that uniform radial InAsP QW formation is possible if conditions are tuned to favor radial growth and suppress the axial growth rate. For instance, a lower temperature and higher V/III ratio is suggested based on the previous growth studies of InP nanowire and nanoshape arrays [9, 32].

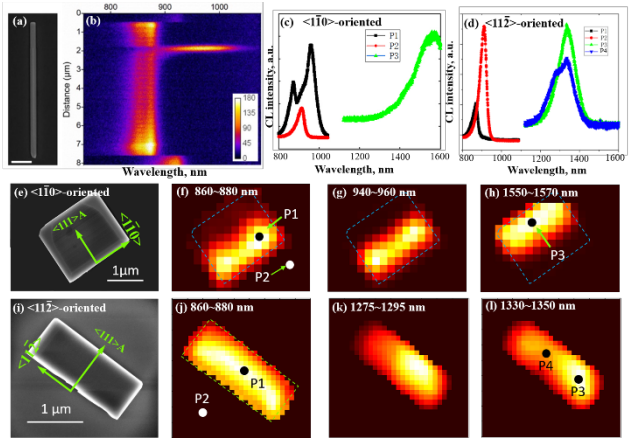

Fig.5 Spatially resolved CL emission for the InAsP/InP QW nanowire and nanomembranes. (a) SEM image of a nanowire together with the CL map (b); (e) and (i) are the $<1\bar{1}0>$- and $<11\bar{2}>$-oriented InP/InAsP QW nanomembrane, respectively. (f-h) and (i-l) are the corresponding normalized intensity maps for the nanomembranes at different wavelength windows. The corresponding CL spectra from each position indicated by points P1-P4 are shown in (c) and (d). The scale bar in (a) is 1 μm.

Conclusions

In conclusion, we demonstrated high-quality InP/InAsP QW growth in both nanowires and nanomembranes. The growth behaviors of InAsP QW were thoroughly studied, including crystal structure, composition, spatial distribution together with the impact on the shape evolution. InAsP QWs grow both axially and laterally, forming ZB and WZ QWs, respectively. Structurally, QW growth along <111> direction can form a different phase (for instance, ZB phase) with respect to the WZ InP matrix while laterally formed QW along all other directions only inherits the crystal stacking sequence of InP. Both axial and lateral QWs present an atomically sharp interface. In terms of composition, growth direction dependent composition difference is observed, reaching as high as 16%. Moreover, there may

exist composition fluctuations in the QW, which leads to a broad emission peak in the CL and photoluminescence (PL) spectra. Axial QW growth rate is reduced due to competitive lateral growth. In <11$\bar{2}$>-oriented nanomembranes, the axial growth rate can be suppressed to nearly zero. Lateral QW distribution varies on different sidewalls. QW formation on the {1$\bar{1}$00} side facets is non-symmetric and non-uniform, growing only on the <11$\bar{2}$>A polar side of the axial ZB QW. This asymmetric QW growth is probably driven by the faster lateral growth rate of ZB QW along <11$\bar{2}$>A polar direction. In comparison, QW grows uniformly on the {11$\bar{2}$0} sidewalls even after 5 QW growth. Emission property from QW in nanowires and <1$\bar{1}$0>-oriented nanomembranes varies from one to another. In comparison, strong and uniform emission at telecommunications wavelength is observed for <11$\bar{2}$>-oriented QW nanomembrane. The growth of subsequent InP layer is strongly affected after InAsP QW growth. First, the axial growth rate of InP is reduced due to the increased lateral growth rate. Secondly, the asymmetric growth deteriorates the symmetry of the nanowires and nanomembranes. The cross-section of InAsP/InP QW nanowire transforms from a hexagonal to a triangular shape. For <1 $\bar{1}$ 0>-orientated nanomembranes, inclined {1 $\bar{1}$ 01} sidewalls are formed after QW growth, forming a “protruding head” at the top.

Our results show that careful growth optimization is required for the growth of InAsP/InP QW nanowires and nanomembranes in order to preserve the symmetry and shapes of the nanostructures, and to obtain a high selectivity between the axial and radial QW growth rate. The revealed growth fundamental of InAsP/InP QW nanowire and nanomembrane provides a good example for other III-V heterostructure fabrication using SAE technique.

Methods

The details of the patterned substrate preparation process by electron beam lithography and reactive ion etching can be found in our previous work.[9] InP/InAsP nanowire arrays were grown in a horizontal Metalorganic Chemical Vapor Deposition (MOCVD, Aixtron 200/4) reactor. Trimethylindium (TMIn), arsine (AsH_3), phosphine (PH_3) were used as precursors for In, As and P elements, respectively. For growth, reactor was heated to 750 °C under the flow of PH_3 and kept for 10 min to desorb possible contaminants. InP nanowires were grown at 730 °C with a TMIn flow rate of 3.373×10^{-6} mol/min and V/III ratio of 172. After InP growth for 16 min, $InAs_{1-x}P_x$ QW was grown for 3 seconds by turning on AsH_3 with an appropriate flow rate to obtain a nominal composition of $InAs_{0.15}P_{0.85}$. Finally, InP was grown again for another 9 min as the top barrier. Other conditions for the QW growth were also investigated and shown in the supporting information (SI).

InP/InAsP QW nanomembranes were grown by a close coupled showerhead (CCS) MOCVD reactor. The InP nanomembrane templates were grown at a surface temperature of 683 °C for 3 min with PH_3 and TMIn at a flow rate of 1.25×10^{-3} and 4.20×10^{-6} mol/min, respectively.[9] A QW with nominal composition of $InAs_{0.3}P_{0.7}$ was then grown at the same condition with AsH_3 flow rate of 5.44×10^{-4} mol/min for 3 seconds, followed by the growth of InP capping layer for another 1.5 min. For multiple QWs, InP barrier layer growth time is reduced to 30 seconds.

The morphology of the nanostructures was characterized using an FEI Verios 460 SEM. A Gatan MonoCL4 Elite CL spectroscopy equipped in the SEM instrument and a commercial micro-Raman system (Renishaw inVia) was used to perform optical characterization. Structural and compositional analyses were performed in an aberration-corrected scanning transmission electron microscope (Cs-STEM) (JEOL JEM-ARM200f) equipped with an energy dispersive X-ray spectroscopy system.

Conflicts of interest

There are no conflicts to declare.

Acknowledgements

National Natural Science Foundation of China (No. 61974166, No. 51702368, No. 61874141); Hunan Provincial Natural Science Foundation of China (2018JJ3684); Open Project of the State Key Laboratory of Luminescence and Applications (SKLA-2018-07); The Australian Research Council (ARC) are acknowledged for financial support. The Australian National Fabrication Facility, ACT Node and the Australian Microscopy and Microanalysis Research Facility are acknowledged for access to facilities used in this work.

Notes and references

1 Wong-Leung, J.; Yang, I.; Li, Z.; Karuturi, S. K.; Fu, L.; Tan, H. H.; Jagadish, C. Engineering iii-v semiconductor nanowires for device applications. *Adv. Mater.* 2019, e1904359.
2 Güniat, L.; Caroff, P.; Fontcuberta i Morral, A. Vapor phase growth of semiconductor nanowires: Key developments and open questions. *Chem. Rev.* 2019, 119, 8958-8971.
3 Noborisaka, J.; Motohisa, J.; Fukui, T. Catalyst-free growth of gaas nanowires by selective-area metalorganic vapor-phase epitaxy. *Appl. Phys. Lett.* 2005, 86, 213102.
4 Mohan, P.; Motohisa, J.; Fukui, T. Controlled growth of highly uniform, axial/radial direction-defined, individually addressable inp nanowire arrays. *Nanotech.* 2005, 16, 2903-2907.
5 Wallentin, J.; Anttu, N.; Asoli, D.; Huffman, M.; Åberg, I.; Magnusson, M. H.; Siefer, G.; Fuss-Kailuweit, P.; Dimroth, F.; Witzigmann, B. et al. Inp nanowire array solar cells achieving 13.8% efficiency by exceeding the ray optics limit. *Science* 2013, 339, 1057-1060.
6 Yao, M.; Cong, S.; Arab, S.; Huang, N.; Povinelli, M. L.; Cronin, S. B.; Dapkus, P. D.; Zhou, C. Tandem solar cells using gaas nanowires on si: Design, fabrication, and observation of voltage addition. *Nano Lett.* 2015, 15, 7217-7224.
7 Guo, W.; Zhang, M.; Banerjee, A.; Bhattacharya, P. Catalyst-free ingan/gan nanowire light emitting diodes grown on (001) silicon by molecular beam epitaxy. *Nano Lett.* 2010, 10, 3355-3359.
8 Chi, C.-Y.; Chang, C.-C.; Hu, S.; Yeh, T.-W.; Cronin, S. B.; Dapkus, P. D. Twin-free gaas nanosheets by selective area growth: Implications for defect-free nanostructures. *Nano Lett.* 2013, 13, 2506-2515.
9 Wang, N.; Yuan, X.; Zhang, X.; Gao, Q.; Zhao, B.; Li, L.; Lockrey, M.; Tan, H. H.; Jagadish, C.; Caroff, P. Shape engineering of inp nanostructures by selective area epitaxy. *ACS Nano* 2019, 13, 7261-7269.
10 Raya, A. M.; Friedl, M.; Martí-Sánchez, S.; Dubrovskii, V. G.; Francaviglia, L.; Alén, B.; Morgan, N.; Tütüncüoglu, G.; Ramasse, Q. M.; Fuster, D. et al. Gaas nanoscale membranes: Prospects for seamless integration of iii–vs on silicon. *Nanoscale* 2020, 12, 815-824.
11 Yeh, T.-W.; Lin, Y.-T.; Ahn, B.; Stewart, L. S.; Dapkus, P. D.; Nutt, S. R. Vertical nonpolar growth templates for light emitting diodes formed with gan nanosheets. *Appl. Phys. Lett.* 2012, 100, 033119.
12 Seidl, J.; Gluschke, J. G.; Yuan, X.; Naureen, S.; Shahid, N.; Tan, H. H.; Jagadish, C.; Micolich, A. P.; Caroff, P. Regaining a spatial dimension: Mechanically transferrable two-dimensional inas nanofins grown by selective area epitaxy. *Nano Lett.* 2019, 19, 4666-4677.
13 Aseev, P.; Fursina, A.; Boekhout, F.; Krizek, F.; Sestoft, J. E.; Borsoi, F.; Heedt, S.; Wang, G.; Binci, L.; Marti-Sanchez, S. et al. Selectivity map for molecular beam epitaxy of advanced iii-v

quantum nanowire networks. *Nano Lett.* 2019, 19, 218-227.
14 Vaitiekėnas, S.; Whiticar, A. M.; Deng, M. T.; Krizek, F.; Sestoft, J. E.; Palmstrøm, C. J.; Marti-Sanchez, S.; Arbiol, J.; Krogstrup, P.; Casparis, L. et al. Selective-area-grown semiconductor-superconductor hybrids: A basis for topological networks. *Phys. Rev. Lett.* 2018, 121, 147701.
15 Aseev, P.; Wang, G.; Binci, L.; Singh, A.; Martí-Sánchez, S.; Botifoll, M.; Stek, L. J.; Bordin, A.; Watson, J. D.; Boekhout, F. et al. Ballistic insb nanowires and networks via metal-sown selective area growth. *Nano Lett.* 2019, 19, 9102-9111.
16 Krogstrup, P.; Ziino, N. L. B.; Chang, W.; Albrecht, S. M.; Madsen, M. H.; Johnson, E.; Nygård, J.; Marcus, C. M.; Jespersen, T. S. Epitaxy of semiconductor–superconductor nanowires. *Nat. Mater.* 2015, 14, 400-406.
17 Deshpande, V.; Djara, V.; O'Connor, E.; Hashemi, P.; Balakrishnan, K.; Caimi, D.; Sousa, M.; Czornomaz, L.; Fompeyrine, J. Dc and rf characterization of ingaas replacement metal gate (rmg) nfets on sige-oi finfets fabricated by 3d monolithic integration. *Solid-State Electron.* 2017, 128, 87-91.
18 Borg, M.; Schmid, H.; Moselund, K. E.; Signorello, G.; Gignac, L.; Bruley, J.; Breslin, C.; Das Kanungo, P.; Werner, P.; Riel, H. Vertical iii–v nanowire device integration on si(100). *Nano Lett.* 2014, 14, 1914-1920.
19 Wirths, S.; Mayer, B. F.; Schmid, H.; Sousa, M.; Gooth, J.; Riel, H.; Moselund, K. E. Room-temperature lasing from monolithically integrated gaas microdisks on silicon. *ACS Nano* 2018, 12, 2169-2175.
20 Oehler, F.; Cattoni, A.; Scaccabarozzi, A.; Patriarche, G.; Glas, F.; Harmand, J. C. Measuring and modeling the growth dynamics of self-catalyzed gap nanowire arrays. *Nano Lett.* 2018, 18, 701-708.
21 Dalacu, D.; Mnaymneh, K.; Wu, X.; Lapointe, J.; Aers, G. C.; Poole, P. J.; Williams, R. L. Selective-area vapor-liquid-solid growth of tunable inasp quantum dots in nanowires. *Appl. Phys. Lett.* 2011, 98, 251101.
22 Ren, D.; Farrell, A. C.; Huffaker, D. L. Axial inas(sb) inserts in selective-area inasp nanowires on inp for optoelectronics beyond 2.5 µm. *Opt. Mater. Express* 2018, 8, 1075-1081.
23 Zhang, Y.; Wu, J.; Aagesen, M.; Holm, J.; Hatch, S.; Tang, M.; Huo, S.; Liu, H. Self-catalyzed ternary core–shell gaasp nanowire arrays grown on patterned si substrates by molecular beam epitaxy. *Nano Lett.* 2014, 14, 4542-4547.
24 Vettori, M.; Piazza, V.; Cattoni, A.; Scaccabarozzi, A.; Patriarche, G.; Regreny, P.; Chauvin, N.; Botella, C.; Grenet, G.; Penuelas, J. et al. Growth optimization and characterization of regular arrays of gaas/algaas core/shell nanowires for tandem solar cells on silicon. *Nanotech.* 2018, 30, 084005.
25 Gazibegovic, S.; Car, D.; Zhang, H.; Balk, S. C.; Logan, J. A.; de Moor, M. W. A.; Cassidy, M. C.; Schmits, R.; Xu, D.; Wang, G. et al. Epitaxy of advanced nanowire quantum devices. *Nature* 2017, 548, 434-438.
26 Car, D.; Wang, J.; Verheijen, M. A.; Bakkers, E. P.; Plissard, S. R. Rationally designed single-crystalline nanowire networks. *Adv. Mater.* 2014, 26, 4875-9.
27 Zhang, G.; Takiguchi, M.; Tateno, K.; Tawara, T.; Notomi, M.; Gotoh, H. Telecom-band lasing in single inp/inas heterostructure nanowires at room temperature. *Sci. Adv.* 2019, 5, eaat8896.
28 Reimer, M. E.; Bulgarini, G.; Akopian, N.; Hocevar, M.; Bavinck, M. B.; Verheijen, M. A.; Bakkers, E.; Kouwenhoven, L. P.; Zwiller, V. Bright single-photon sources in bottom-up tailored nanowires. *Nat. Commun.* 2012, 3.
29 Karimi, M.; Jain, V.; Heurlin, M.; Nowzari, A.; Hussain, L.; Lindgren, D.; Stehr, J. E.; Buyanova, I. A.; Gustafsson, A.; Samuelson, L. et al. Room-temperature inp/inasp quantum discs-in-nanowire infrared photodetectors. *Nano Lett.* 2017, 17, 3356-3362.
30 Staudinger, P.; Moselund, K. E.; Schmid, H. Exploring the size limitations of wurtzite iii-v film growth. *Nano Lett.* 2020, 20, 686-693.
31 Staudinger, P.; Mauthe, S.; Triviño, N. V.; Reidt, S.; Moselund, K. E.; Schmid, H. Wurtzite inpmicrodisks: From epitaxy to room-temperature lasing. arXiv:2004.10677 2020.
32 Gao, Q.; Saxena, D.; Wang, F.; Fu, L.; Mokkapati, S.; Guo, Y.; Li, L.; Wong-Leung, J.; Caroff, P.; Tan, H. H. et al. Selective-area epitaxy of pure wurtzite inp nanowires: High quantum efficiency and room-temperature lasing. *Nano Lett.* 2014, 14, 5206-5211.
33 Gibson, S. J.; van Kasteren, B.; Tekcan, B.; Cui, Y.; van Dam, D.; Haverkort, J. E. M.; Bakkers, E. P. A. M.; Reimer, M. E. Tapered inp nanowire arrays for efficient broadband high-speed single-photon detection. *Nat. Nanotechnol.* 2019, 14, 473-479.
34 Gautam, V.; Naureen, S.; Shahid, N.; Gao, Q.; Wang, Y.; Nisbet, D.; Jagadish, C.; Daria, V. R. Engineering highly interconnected neuronal networks on nanowire scaffolds. *Nano Lett.* 2017, 17, 3369-3375.
35 Xu, W.-Z.; Ren, F.-F.; Jevtics, D.; Hurtado, A.; Li, L.; Gao, Q.; Ye, J.; Wang, F.; Guilhabert, B.; Fu, L. et al. Vertically emitting indium phosphide nanowire lasers. *Nano Lett.* 2018, 18, 3414-3420.
36 Kornienko, N.; Gibson, N. A.; Zhang, H.; Eaton, S. W.; Yu, Y.; Aloni, S.; Leone, S. R.; Yang, P. Growth and photoelectrochemical energy conversion of wurtzite indium phosphide nanowire arrays. *ACS Nano* 2016, 10, 5525-35.
37 Yang, I.; Zhang, X.; Zheng, C.; Gao, Q.; Li, Z.; Li, L.; Lockrey, M. N.; Nguyen, H.; Caroff, P.; Etheridge, J. et al. Radial growth evolution of ingaas/inp multi-quantum-well nanowires grown by selective-area metal organic vapor-phase epitaxy. *ACS Nano* 2018, 12, 10374-10382.
38 Han, Y.; Ng, W. K.; Ma, C.; Li, Q.; Zhu, S.; Chan, C. C. S.; Ng, K. W.; Lennon, S.; Taylor, R. A.; Wong, K. S. et al. Room-temperature inp/ingaas nano-ridge lasers grown on si and emitting at telecom bands. *Optica* 2018, 5, 918-923.
39 Mohan, P.; Motohisa, J.; Fukui, T. Fabrication of inp ⁄ inas ⁄ inp core-multishell heterostructure nanowires by selective area metalorganic vapor phase epitaxy. *Appl. Phys. Lett.* 2006, 88, 133105.
40 Tateno, K.; Zhang, G.; Gotoh, H.; Sogawa, T. Vls growth of alternating inasp/inp heterostructure nanowires for multiple-quantum-dot structures. *Nano Lett.* 2012, 12, 2888-93.
41 Kuyanov, P.; LaPierre, R. R. Photoluminescence and photocurrent from inp nanowires with inasp quantum dots grown on si by molecular beam epitaxy. *Nanotech.* 2015, 26, 315202.
42 Dalacu, D.; Mnaymneh, K.; Lapointe, J.; Wu, X.; Poole, P. J.; Bulgarini, G.; Zwiller, V.; Reimer, M. E. Ultraclean emission from inasp quantum dots in defect-free wurtzite inp nanowires. *Nano Lett.* 2012, 12, 5919-23.
43 Zhong, Z.; Li, X.; Wu, J.; Li, C.; Xie, R. B.; Yuan, X.; Niu, X.; Wang, W.; Luo, X.; Zhang, G. et al. Wavelength-tunable inasp quantum dots in inp nanowires. *Appl. Phys. Lett.* 2019, 115, 053101.
44 Göransson, D. J. O.; Heurlin, M.; Dalelkhan, B.; Abay, S.; Messing, M. E.; Maisi, V. F.; Borgström, M. T.; Xu, H. Q. Coulomb blockade from the shell of an inp-inas core-shell nanowire with a triangular cross section. *Appl. Phys. Lett.* 2019, 114, 053108.
45 Yang, I.; Li, Z.; Wong-Leung, J.; Zhu, Y.; Li, Z.; Gagrani, N.; Li, L.; Lockrey, M. N.; Nguyen, H.; Lu, Y. et al. Multiwavelength single nanowire ingaas/inp quantum well light-emitting diodes. *Nano Lett.* 2019, 19, 3821-3829.
46 Ishizaka, F.; Hiraya, Y.; Tomioka, K.; Motohisa, J.; Fukui, T. Growth of all-wurtzite inp/alinp core–multishell nanowire array. *Nano Lett.* 2017, 17, 1350-1355.
47 Yuan, X.; Caroff, P.; Wang, F.; Guo, Y.; Wang, Y.; Jackson, H. E.; Smith, L. M.; Tan, H. H.; Jagadish, C. Antimony induced {112}a faceted triangular gaas1−xsbx/inp core/shell nanowires and their enhanced optical quality. *Adv. Funct. Mater.* 2015, 25, 5300-5308.
48 Kempa, T. J.; Kim, S.-K.; Day, R. W.; Park, H.-G.; Nocera, D. G.; Lieber, C. M. Facet-selective growth on nanowires yields multi-component nanostructures and photonic devices. *J.Am.Chem.Soc.* 2013, 135, 18354-18357.
49 Yuan, X.; Yang, J.; He, J.; Tan, H. H.; Jagadish, C. Role of surface energy in nanowire growth. Journal of Physics D: *Appl. Phys.* 2018,

51, 283002.
50 Paladugu, M.; Zou, J.; Guo, Y.-N.; Zhang, X.; Joyce, H. J.; Gao, Q.; Tan, H. H.; Jagadish, C.; Kim, Y. Polarity driven formation of inas/gaas hierarchical nanowire heterostructures. *Appl. Phys. Lett.* 2008, 93, 201908.